Electronic Supplementary Material (ESI) for CrystEngComm.

Supporting Information

A facile method to enhance the output performance of triboelectric nanogenerators based on coordination polymers by modulating terminal coordination groups

Wenjie Wang,[a] Ying-Ying Zhang,*[a] Sheng Zhang,[a] Chao Huang*[a] and Liwei Mi*[a]

Table of contents

1. Experiment Section

1.1 Materials

All the chemical reagents in this work are obtained from commercial and can be used without make further of purification.

1.2 Syntheses of Compounds 1-3

Synthesis of [Cu(μ_3-H_3ttc)Cl]$_n$ (1). Solid CuCl (0.0371 g, 0.375 mmol) and H_3ttc (0.0222 g, 0.125 mmol) were dissolved in CH_3CN (20 ml) and CH_2Cl_2 (15 ml), respectively. CuCl solution (4 ml) and H_3ttc solution (3 ml) were separated by 2 ml buffer (the mixed solvent of CH_2Cl_2 and CH_3CN in the volume ratio of 1:1). The test tube was sealed with preservative film and allowed to stand at room temperature for 5 days to obtain orange red bulk crystals. Yield: 43% based on CuCl. Elemental analysis calcd (%) for $Cu_3C_3N_3S_3Cl_3$: C, 13.04; H, 1.09; N, 15.21. Found: C, 13.03; H, 1.08; N, 15.23. IR (KBr pellets, ν/cm^{-1}): 3448(s), 2857(w), 1529(s), 1388(m), 1238(w), 1129(s), 806(w), 597(w), 462(w).

Synthesis of [Cu(μ_3-H_3ttc)Br]$_n$ (2). The synthetic procedure of 2 was similar to that of 1 by using CuBr instead of CuCl, giving orange red bulk crystals. Yield: 49% based on CuBr. Elemental analysis calcd (%) for $Cu_3C_3N_3S_3Br_3$: C, 11.24; H, 0.94; N, 13.10. Found: C, 11.15; H, 0.92; N, 13.02. IR (KBr pellets, ν/cm^{-1}): 3448(m), 3050(w), 2856(w), 1637(w), 1535(s), 1386(m), 1127(s)，787(w), 594(w), 462(w).

Synthesis of [Cu(μ_3-H_3ttc)I]$_n$ (3). The synthetic procedure of **3** was similar to that of **1** by using CuI instead of CuCl, giving orange red bulk crystals. Yield: 41% based on CuI. Elemental analysis calcd (%) for $Cu_3C_3N_3S_3I_3$: C, 9.80; H, 0.82; N, 11.43. Found: C, 9.82; H, 0.80; N, 11.45. IR (KBr pellets, ν/cm^{-1}):, 3442(w), 2993(w), 2878(m), 1562(s), 1378(s), 1259(s), 1120(s), 764(m), 463(w).

1.3 Fabrication of 1/2/3-based TENG

An appropriate amount of compounds **1-3** were evenly coated on 5 cm × 5 cm copper tape after full grinding and the copper line was fixed on the other side of the copper tape by using silver epoxy resin. Polyvinylidene fluoride (PVDF) prepared was used as the counter electrode.[1,2]

2. The working principle of the assembled TENGs

Fig. S6(i) reveals the initial state of potential difference in external circuit without external force. Under the action of external force, the two electrodes contact each other that makes equal but opposite charges generated in PVDF and compound layer. The PVDF layer was negatively charges relative to the compound layer (Fig. S6(ii)). When the external force is removed, the potential difference between the upper and lower electrodes will be generated due to electrostatic induction, which makes the electrons flow from the compound layer to the PVDF electrode (Fig. S6(iii)). The current will not be detected in the external circuit with the charge reaches the balance again (Fig. S6(iv)). The potential difference decreases with the decrease of the distance between the two electrodes when the external force is applied again, so that electrons flow from the PVDF electrode to the compound layer (Fig. S6(v)), until the charge accumulation reaches a new charge balance (Fig. S6(ii)).

3. Characterizations

FI-IR spectra were performed with KBr particles of 400-4000cm^{-1} on thermal is50FT- IR. Powder X-ray diffraction patterns (PXRD) were taken from by Bruker D8 advanced X-ray powder diffractometer with Cu-kα irradiation. Thermo Scientific K-Alpha X-ray photoelectron spectroscopy with Al-Kα X-rays source obtained X-ray photoelectron spectroscopy (XPS) spectra. The morphology, size and elemental composition of the samples were observed by using Zeiss Merlin compact field emission scanning electron microscope (FE-SEM) equipped with an energy-dispersive

X-ray spectroscopy (EDS) system. The dielectric constant and dielectric loss of the compound were measured by an impedance analyzer (Agilent 4294A) in the frequency range of 10^3-10^7. I_{sc} and V_o are measured by a SR570 low-noise current amplifier (Stanford Research System) and 2657A HIGH POWER SYSTEM Source Meter, respectively. The charging curves of 0.22, 1 and 2.2 μF commercial capacitors were obtained by the electrochemical workstation (Zennium-Pro 43138). The charge-discharge profile of the 100 μF capacitor were monitored by the electrochemical workstation (CHI660E, Shanghai Chenhua Instrument Co., Ltd, China). The surface morphology of carbon steel after 0 h, 1 h, 3 h, 5 h and 7 h was observed by 4X metallographic microscope. The electrochemical measurements of carbon steel with and without the **I**-TENG were carried out by CHI 660E in a three-electrode system, and the carbon steel, platinum foil, and saturated calomel electrode (SCE) were used as the working electrode, counter electrode, and reference electrode, respectively.

4. Figures and Tables

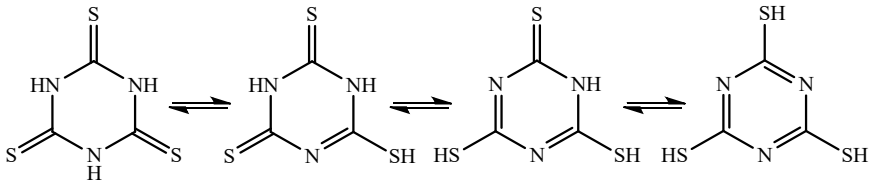

A **B** **C** **D**

Scheme S1. Structures of H_3ttc.

Table S1. Crystallographic data and structure refinement parameters for compounds **1-3**.[3]

Complex	**1**	**2**	**3**
empirical formula	$C_3H_3N_3S_3CuCl$	$C_3H_3N_3S_3CuBr$	$C_3H_3N_3S_3CuI$
T[K]	293	293	293
Mr	276.25	320.71	367.70
crystal system	cubic	cubic	cubic
space group	$Pa\ \bar{3}$	$Pa\ \bar{3}$	$Pa\ \bar{3}$
a [Å]	11.7472(4)	11.8847(3)	12.0266(4)
b [Å]	11.7472(4)	11.8847(3)	12.0266(4)
c [Å]	11.7472(4)	11.8847(3)	12.0266(4)
α [°]	90	90	90
β [°]	90	90	90
γ [°]	90	90	90
V [Å^3]	1621.07(10)	1678.67(7)	1739.52(10)
Z	8	8	8
ρ_{calc} (g cm^{-3})	2.264	2.538	2.808
μ [mm^{-1}]	3.726	8.040	6.715
F(000)	1088	1232	1376
θ range [°]	3.00 to 27.82	2.97 to 27.84	2.93 to 27.85
collected reflns	9510	9865	9933
unique reflns	651	671	698
goodness of fit	1.143	1.344	1.314
R_1/wR_2 [I >2σ(I)][a]	0.0223 / 0.0568	0.0392 / 0.0866	0.0836 / 0.1880
R_1/wR_2 (all data)[a]	0.0237 / 0.0574	0.0411 / 0.0872	0.0865 / 0.1894

[a] $R_1=\Sigma||F_0|-|F_c||$ (based on reflections with $F_0^2>2\sigma F^2$). $wR_2=[\Sigma[w(F_0^2-F_c^2)^2]/\Sigma[w(F_0^2)^2]]^{1/2}$; $w=1/[\sigma^2(F_0^2)+(0.095P)^2]$; $P=[\max(F_0^2, 0)+2F_c^2]/3$(also with $F_0^2>2\sigma F^2$)

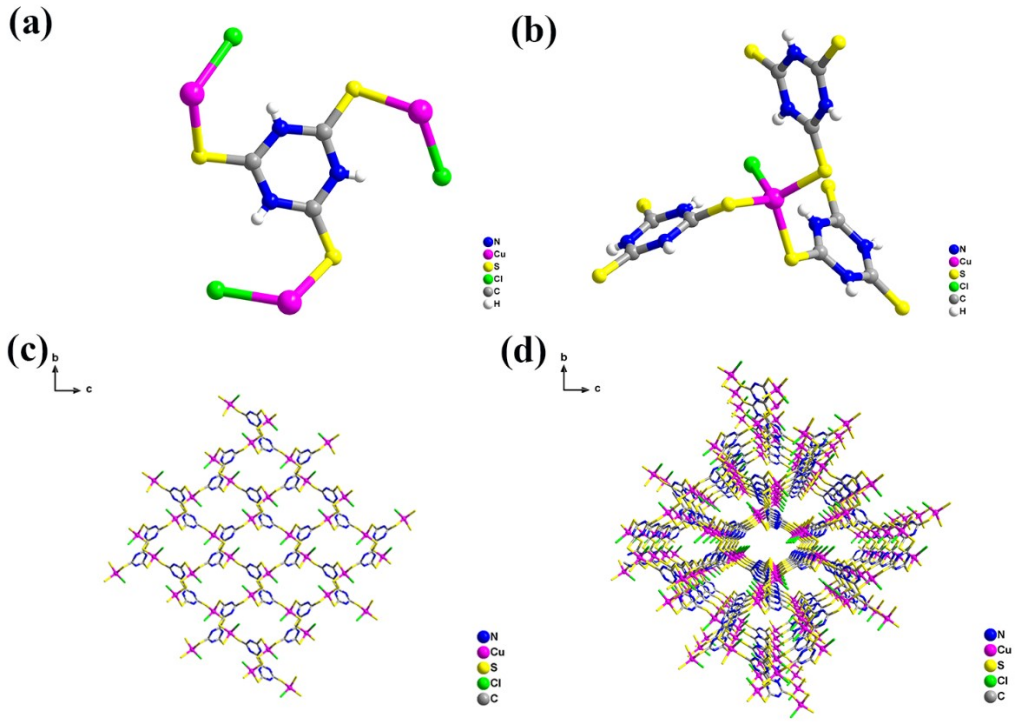

Fig. S1. (a) Coordination mode of the ligand H_3ttc and (b) coordination environment of metal centers in compound **1**. (c) The single-layer and (d) three-dimensional structure of compound **1** viewed along *a* axis. Hydrogen atoms were omitted for clarity.

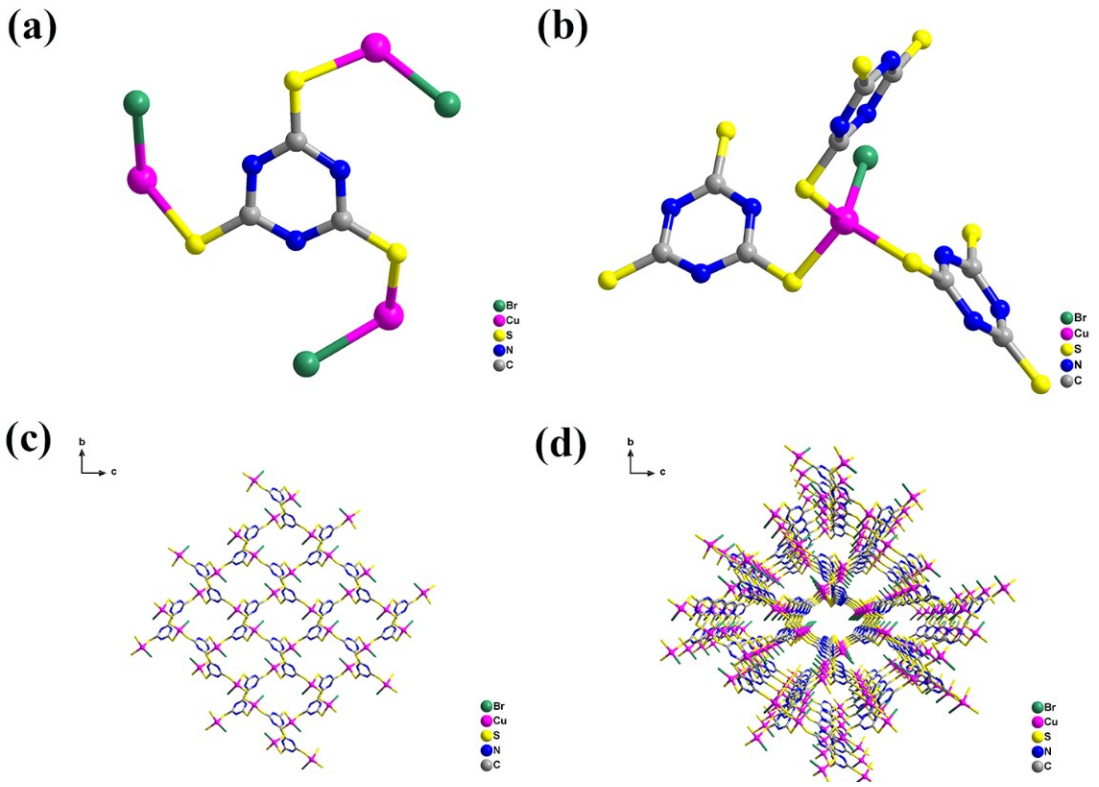

Fig. S2. (a) Coordination mode of the ligand H_3ttc and (b) coordination environment of metal centers in compound **2**. (c) The single-layer and (d) three-dimensional structure of compound **2** viewed along *a* axis. Hydrogen atoms were omitted for clarity.

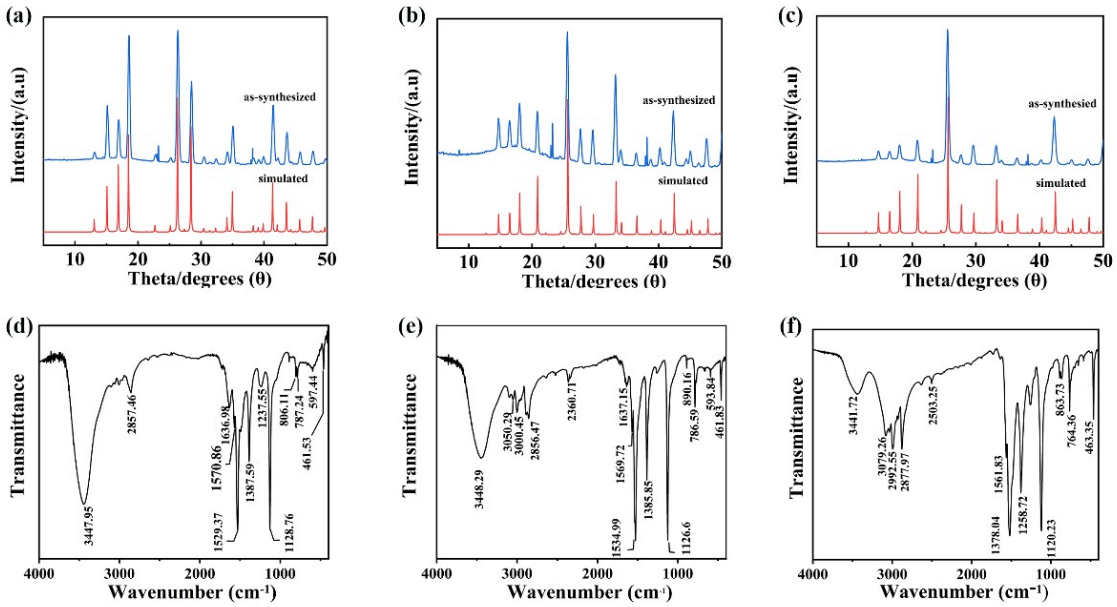

Fig. S3. (a-c) PXRD spectra of compounds **1**-**3**. (d-f) FT-IR spectra of compounds **1**-**3**.

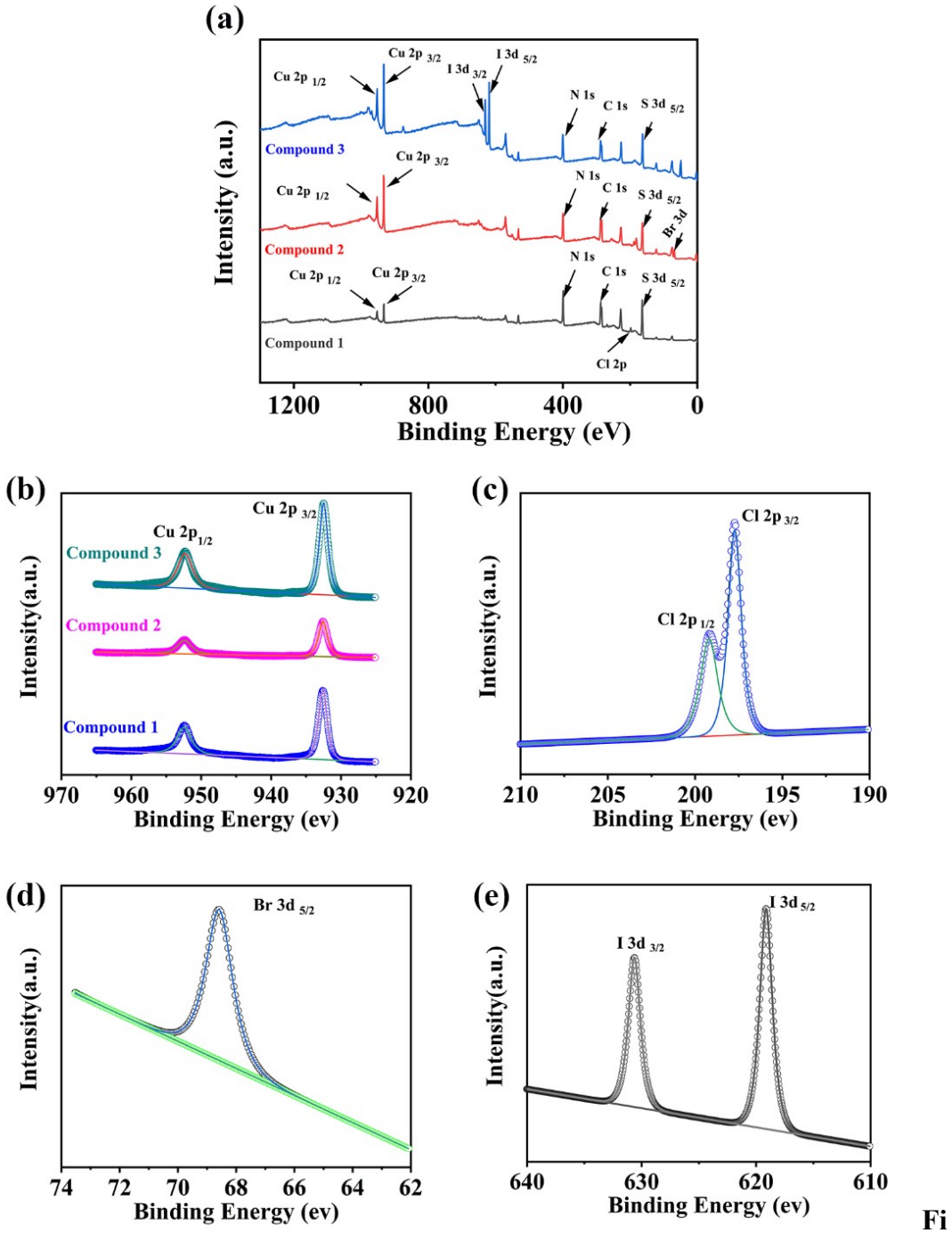

Fig. S4. (a) The XPS spectra of compounds **1-3**. (b-e) The high-resolution Cu 2p, Cl 2p, Br 3d and I 3d XPS spectra of compounds **1-3**.

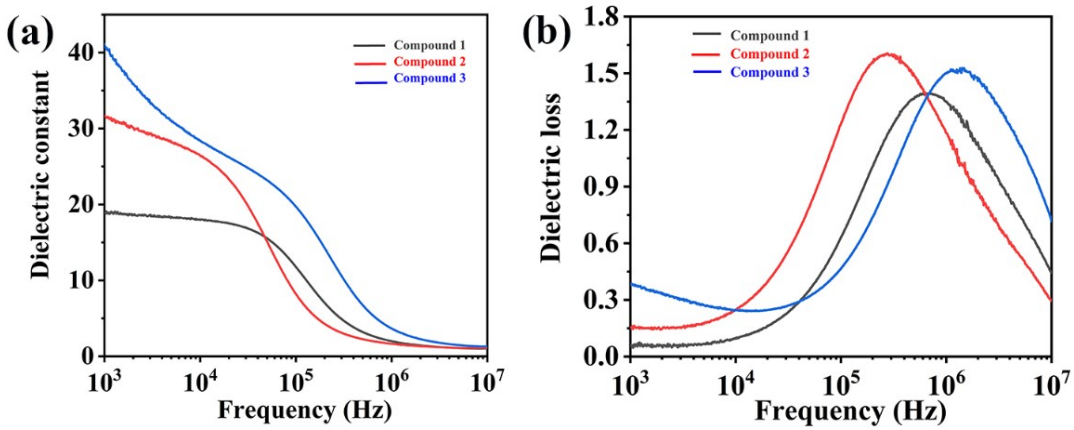

Fig. S5. (a) Dielectric constant and (b) dielectric loss of compounds **1-3**.

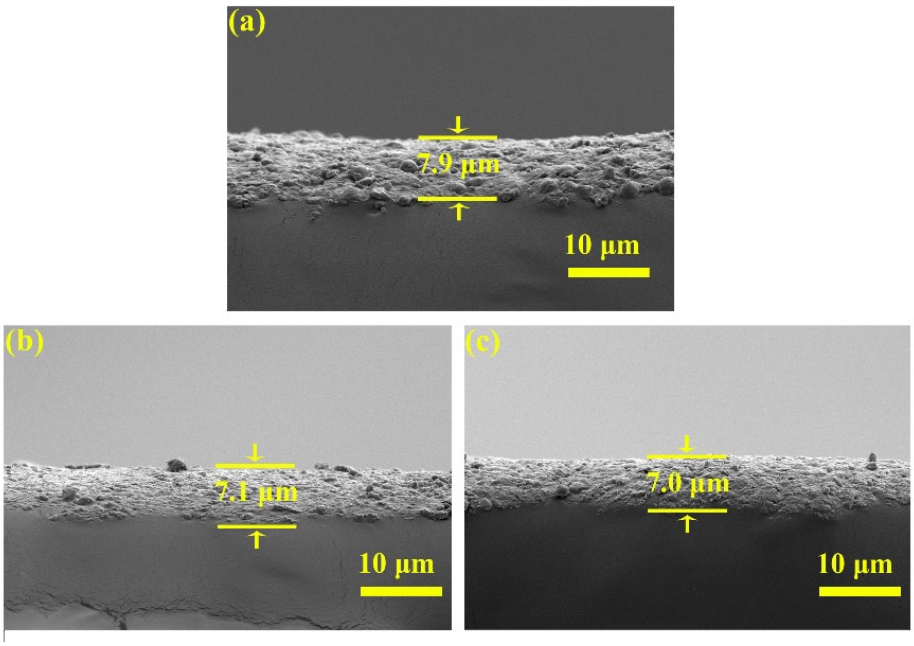

Figure S6. Cross-sectional SEM images of films (a) **1**, (b) **2** and (c) **3** on the Cu layer.

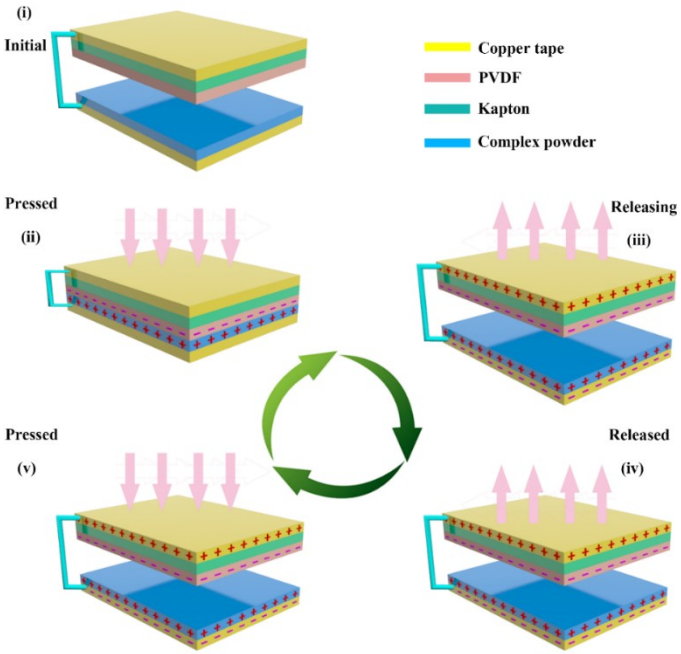

Fig. S7. Working principle of CP-based TENGs.

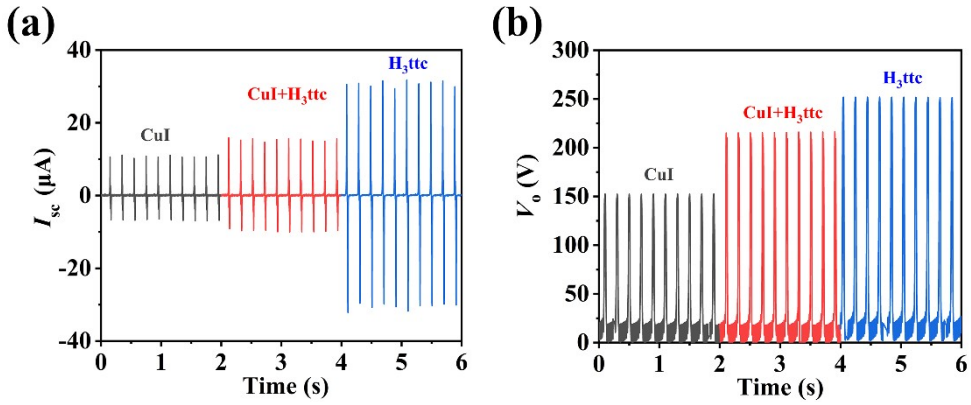

Fig. S8. (a) I_{sc} and (b) V_o of CuI-TENG, Mix-TENG and L-TENG.

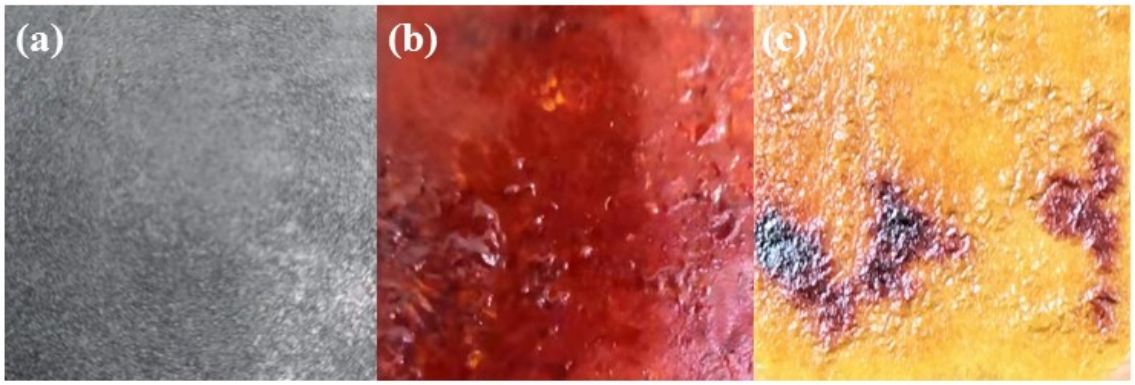

Fig. S9. Photos of I_2 layer after just coating (a), after working for 0.5 h (b) and after standing for 8 h (c).

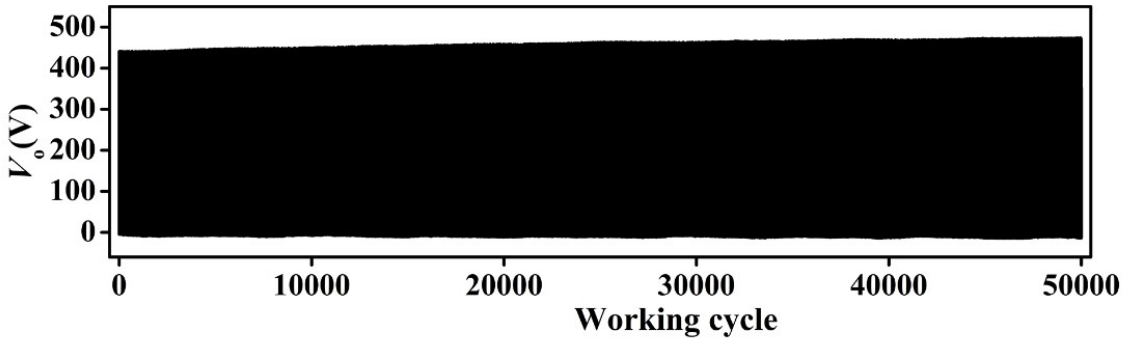

Fig. S10. V_o of **I**- TENG after working 50,000 cycles.

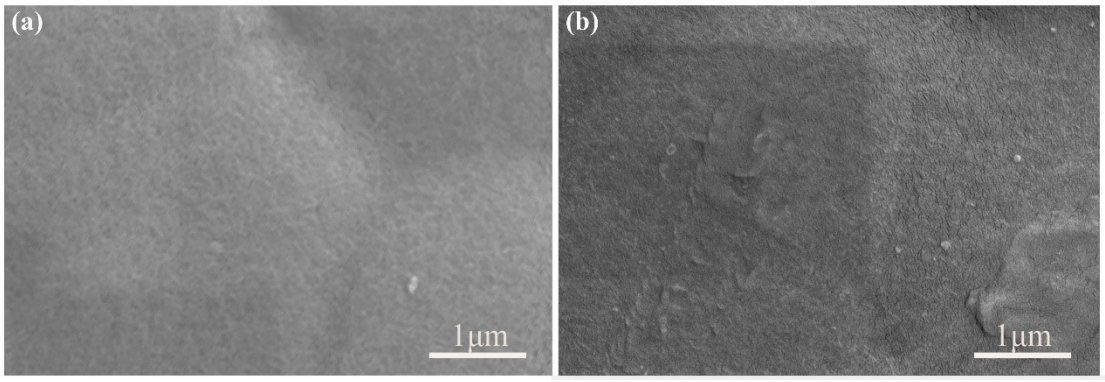

Fig. S11. FE-SEM images of PVDF-based friction layer before (a) and after (b) testing.

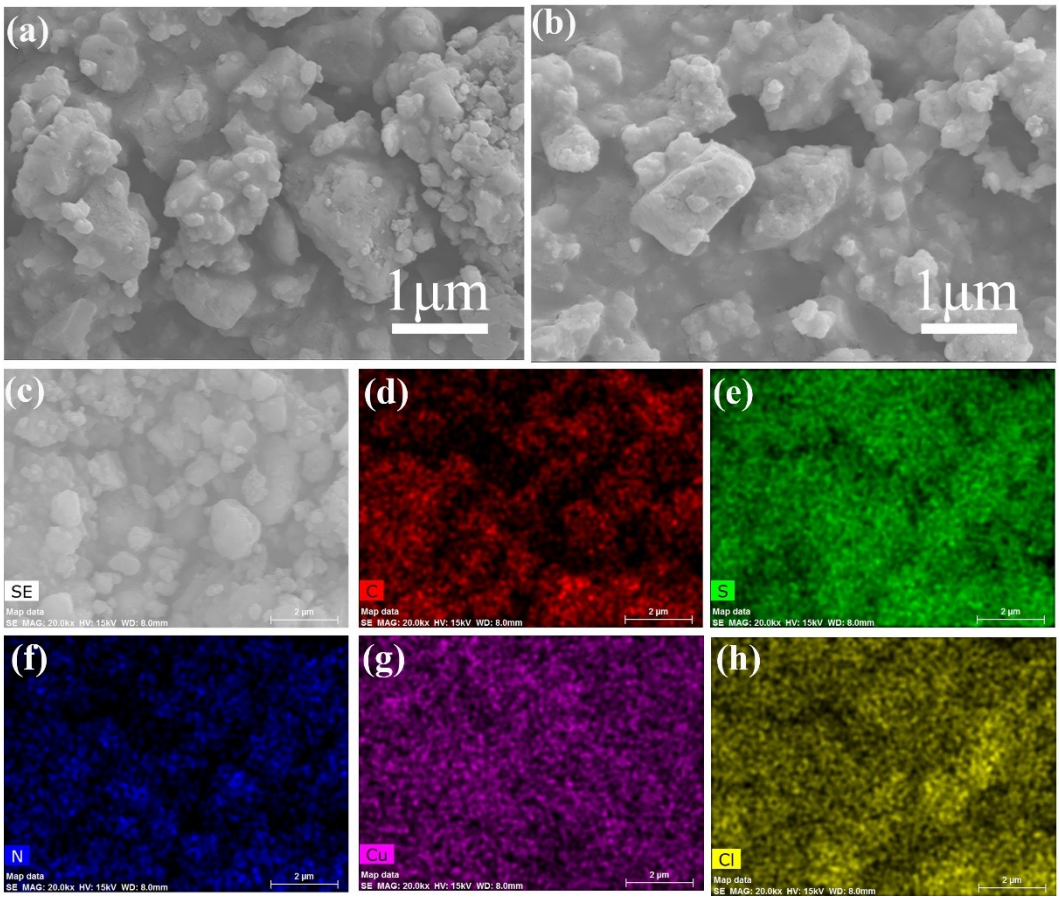

Fig. S12. (a,b) FE-SEM images of compound **1**-based friction layer before (a) and after (b) testing. (c-h) EDS mapping analysis of C, S, N, Cu and Cl in compound **1**.

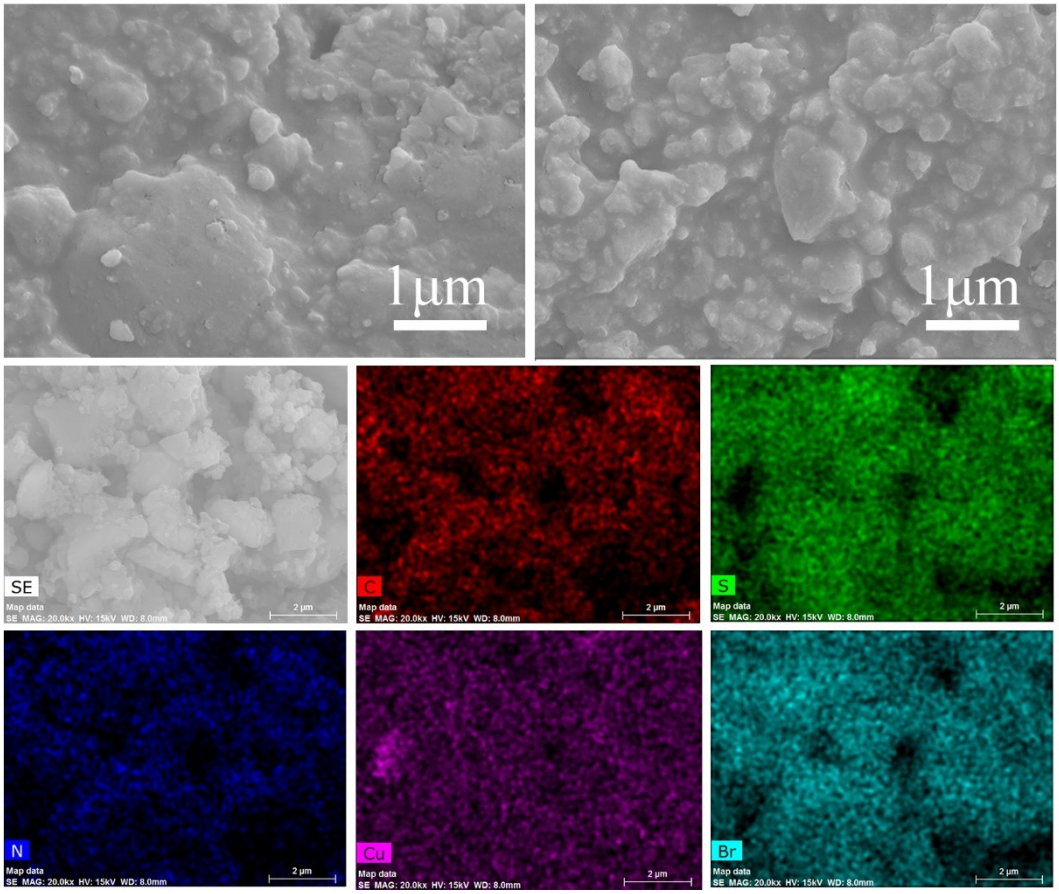

Fig. S13. (a,b) FE-SEM images of compound **2**-based friction layer before (a) and after (b) testing. (c-h) EDS mapping analysis of C, S, N, Cu and Br in compound **2**.

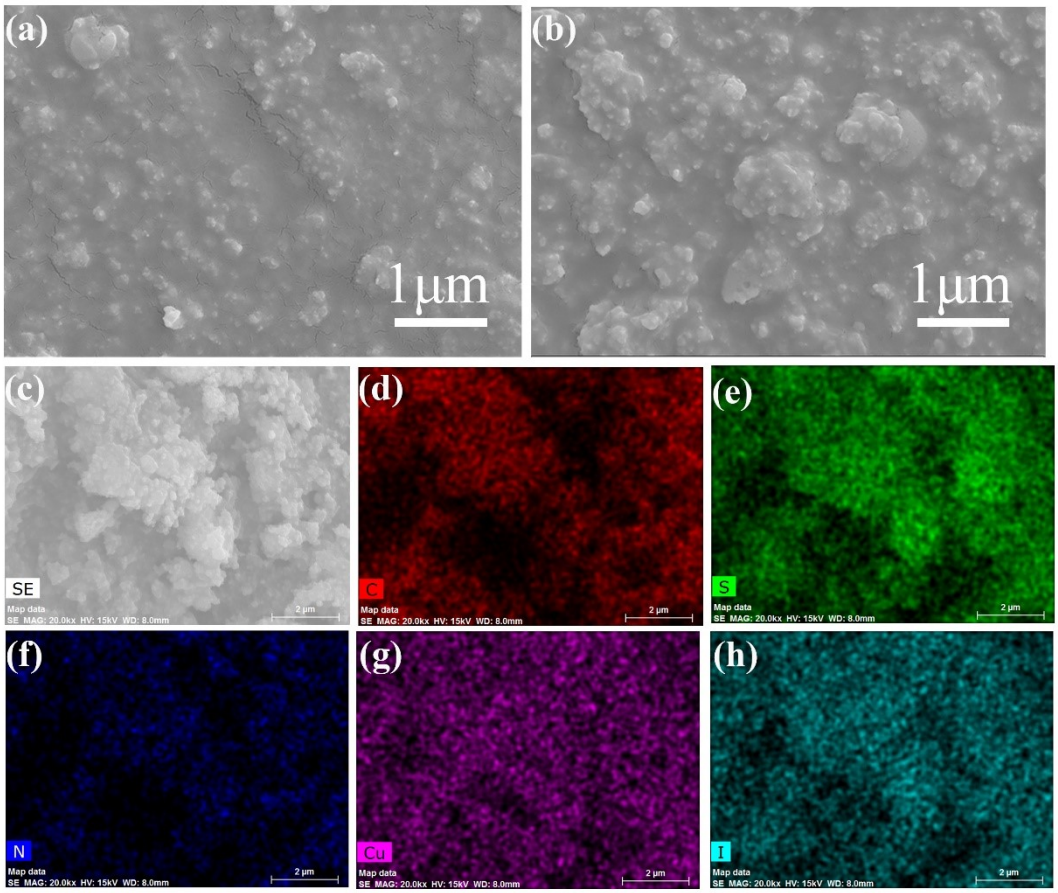

Fig. S14. (a,b) FE-SEM images of compound **3**-based friction layer before (a) and after (b) testing. (c-h) EDS mapping analysis of C, S, N, Cu and I in compound **3**.

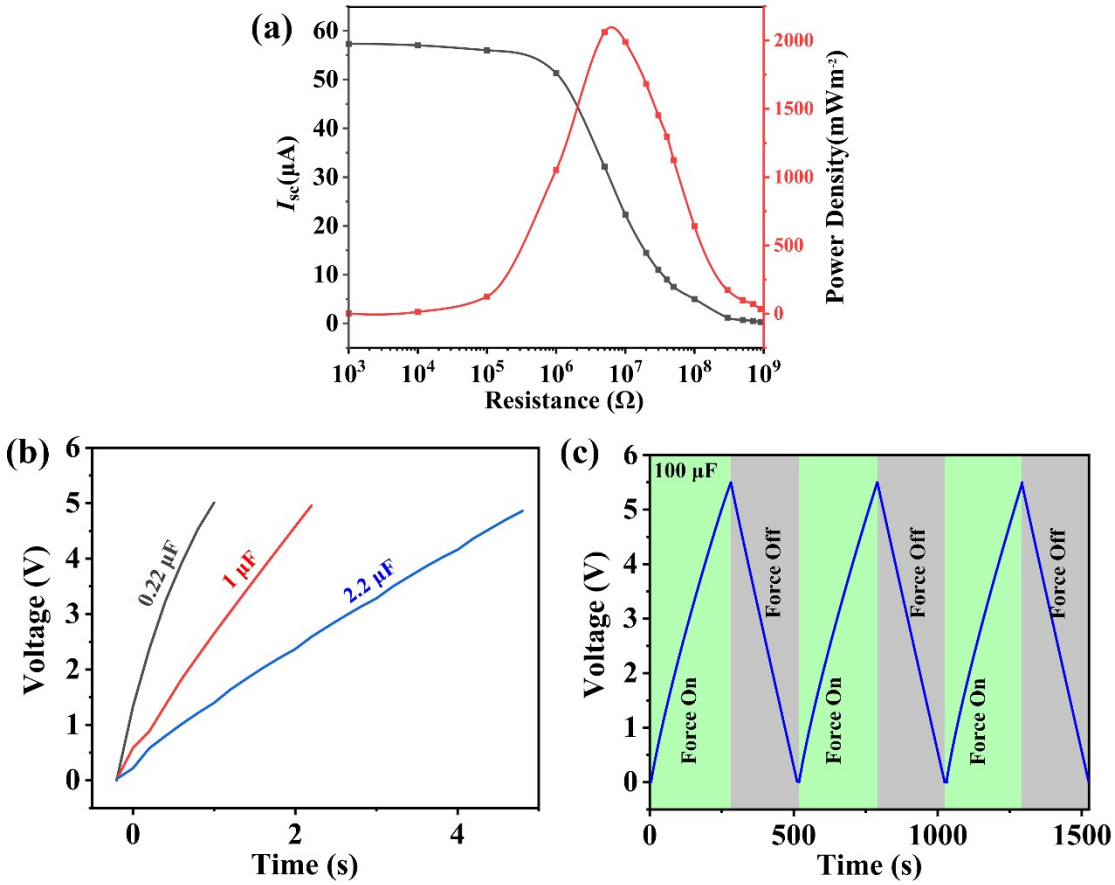

Fig. S15. (a) The output current and power density of **I**-TENG under different loads resistance. (b) The charging curves of 0.22 μF, 1μF, 2.2 μF capacitors by using **I**-TENG. (c) The charge-discharge cycles of a 100 μF capacitor.

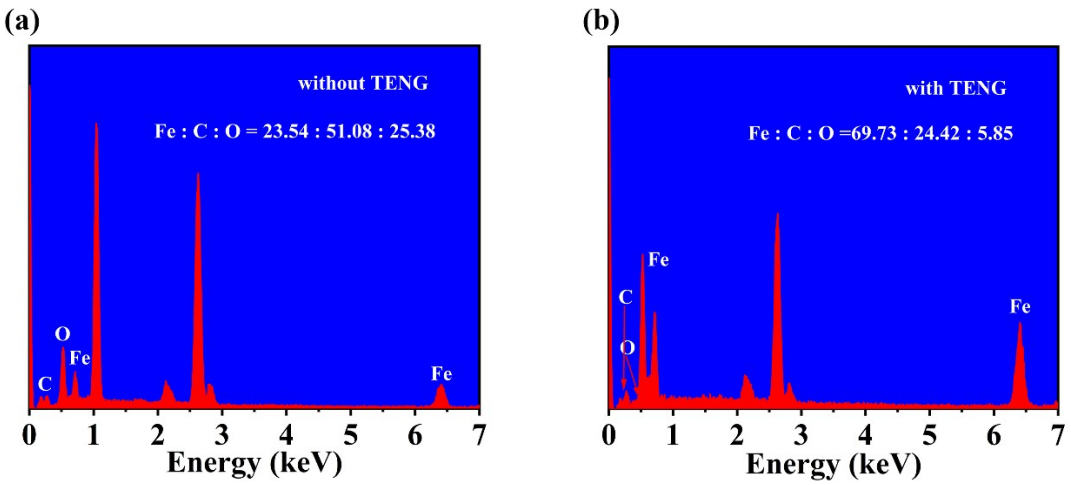

Fig. S16. The EDS spectra of the corrosion products on the surface of carbon steels connected (a) with and (b) without TENG.

5. References

1. Z. Wang, L. Cheng, Y.B. Zheng, Y. Qin and Z. L. Wang, *Nano. Energy*, 2014, **10**, 37-43.

2. W. X. Guo, X.Y. Li, M.X. Chen, L. Xu, L. Dong, X. Cao, W. Tang, J. Zhu, C.J. Lin, C.F. Pan and Z. L. Wang, *Adv. Funct. Mater*, 2014, **24**, 6691-6699.

3. D. Li, W.-J. Shi and L. Hou, *Inorg. Chem.*, 2005, **44**, 3907-3913.